Dynamics of metal foam deformation during Taylor cylinder–Hopkinson bar impact experiment

Sergey L. Lopatnikov [a,b], Bazle A. Gama [a,c,*], Md. Jahirul Haque [a], Carl Krauthauser [a], John W. Gillespie Jr. [a,b,c], Mustafa Guden [d], Ian W. Hall [a,e]

[a] Center for Composite Materials, University of Delaware, Newark, DE 19716, USA
[b] Department of Civil and Environmental Engineering, University of Delaware, Newark, DE 19716, USA
[c] Department of Materials Science and Engineering, University of Delaware, Newark, DE 19716, USA
[d] Department of Mechanical Engineering, Izmir Institute of Technology, Gulbahce 35437 Urla-Izmir, Turkey
[e] Department of Mechanical Engineering, University of Delaware, Newark, DE 19716, USA

Abstract

Analytical solutions for dynamic deformation of foam materials during the Taylor cylinder–Hopkinson bar impact experiment were obtained. It was shown that shock wave of foam collapse appears during the fast impact. The results of this experiment can be used in estimating the average material properties of the foam under dynamic loading conditions. Results show that the undeformed and change in length of foam specimens are in good agreement between theory and experiment, as well as numerical analysis.

© 2003 Published by Elsevier Science Ltd.

1. Introduction

Closed-cell metal foams have unique non-linear deformation behavior, which make them attractive in many applications. The building block of this family of cellular material is a polyhedron shell of different sizes and wall thicknesses, and usually filled with a gas such as air. Under quasi-static deformation, metal foam shows three distinct regions of deformation (Fig. 1). In the first region, elastic deformation of the cell walls appears on the engineering stress–strain diagram as the elastic region. The buckling and plastic collapse of foam cells appear as the quasi-plateau region (Region 2). After the collapse of the foam cells, densification of the foam makes it stiffer as it approaches the density of its constituent material (Region 3). The non-linear behavior of foam materials is often characterized by different parameters. The critical strain and stress (ε_{cr}, σ_{cr}) is defined at the intersection of tangents drawn in the linear-elastic and quasi-plateau region on the engineering stress–strain plot. Similarly, the densification or locking strain (ε_d) is defined at the intersection of tangents

drawn in the quasi-plateau and densification region and is presented in Fig. 1 [1]. The energy absorbed per unit volume of foam material, U_{max}^{Q-S}, during quasi-static compression can be expressed as:

$$U_{max}^{Q-S} = \int_0^{\varepsilon_{max}^{Q-S}} \sigma \, d\varepsilon \qquad (1)$$

where, ε_{max}^{Q-S}, is the maximum strain obtained from quasi-static compression. An elastic-perfectly-plastic-rigid (E-P-P-R) model of foam material, which gives the same energy absorbed per unit volume of foam material, can be defined with three parameters ε_{cr}^P, σ_{cr}^P, and ε_{max}, where, $\varepsilon_{max} = 1 - (\rho_0/\rho_a)$, and the critical stress of E-P-P-R model, $\sigma_{cr}^P = E\varepsilon_{cr}^P$, can be estimated from the following expression:

$$\frac{(\sigma_{cr}^P)^2}{2E} - \varepsilon_{max}\sigma_{cr}^P + U_{max}^{Q-S} \simeq 0 \qquad (2)$$

Fig. 1 shows this model as a dotted line, and may be used in the analytical formulation of foam compression. This model is conservative in energy absorption; however, it is non-conservative in elastic deformation. Because the elastic deformation is relatively small, this model is suitable for describing the energy absorbing behavior of foam materials. The non-linear large deformation and energy absorbing characteristics of foam

---
* Corresponding author. Address: Center for Composite Materials, University of Delaware, Newark, DE 19716, USA.
E-mail address: gama@ccm.udel.edu (B.A. Gama).

Nomenclature

|			
ε	strain	t	time
ε_{cr}	critical strain	u	parameter
ε_{cr}^{P}	critical strain in E-P-P-R model	v_{f0}	volume fraction of densified foam
ε_{d}	densification/locking strain	x	coordinate in the impact direction
ε_{max}	maximum strain at complete densification	A	constant
ε_{max}^{Q-S}	maximum strain obtained from quasi-static compression	B	constant
		C	velocity of the shock front
ε_{V}	strain gage voltage	C_1	constant
v_{a}	Poisson's ratio of aluminum	E_0	elastic modulus of aluminum foam
v_{B}	Poisson's ratio of the Hopkinson bar material	E_a	elastic modulus of aluminum
ρ_0	density of aluminum foam	E_B	elastic modulus of Hopkinson bar material
ρ_a	density of aluminum	G_g	amplification factor
ρ_B	density of the Hopkinson bar material	K_g	strain gage factor
ρ_d	density of aluminum foam at ε_d	L_0	initial length of the foam specimen
σ	stress	L	length of the un-collapsed foam
σ^*	stress in the densified foam	L_{cr}	critical length of the un-collapsed foam
σ_{cr}	critical stress	ΔL	change in length
σ_{cr}^{P}	critical stress in E-P-P-R model	U_{max}^{Q-S}	absorbed energy per unit volume of foam material at ε_{max}^{Q-S}
σ_{y}^{a}	yield stress of aluminum		
τ_0	dimensionless initial time	V_0	initial velocity of foam specimen
c_0	elastic wave speed of aluminum foam	V	velocity of the foam specimen
s	dimensionless length parameter	V_I	bridge input voltage
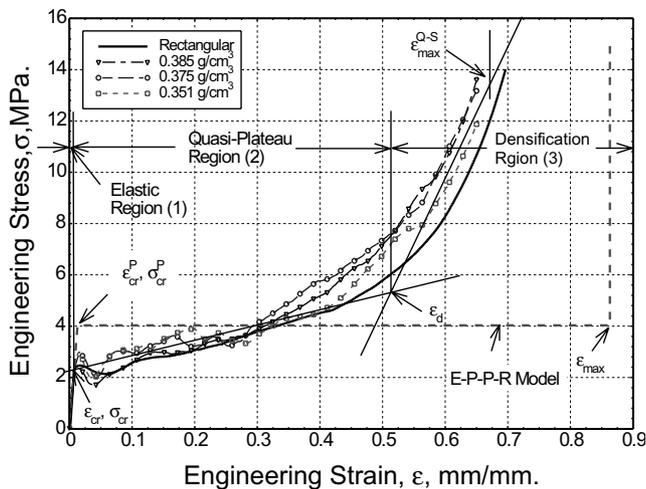
Fig. 1. Quasi-static compression behavior of metal foams.

materials can be used in applications where impact energy absorption and shock attenuation is important. Thus, the physical mechanisms of dynamic deformation and energy absorption during non-quasi-static impact problems need to be investigated.

In a previous work of the authors [2], the high-velocity impact of a massive plate on a metal foam layer was considered, and through analytical and numerical study it was identified that a shock wave of foam collapse appears. A quasi-static regime and three different high impact velocity regimes were identified, out of which two high velocity regimes are of engineering interest. Shock wave propagation is important in all three high velocity regimes. In one of the latter regimes, the shock wave propagates through a completely non-perturbed medium; and in the other, an elastic precursor with amplitude in the range of the critical stress appears. This acoustic precursor propagates with the linear sound velocity and as a result, the shock front propagates through a dynamically perturbed material. It was also shown that the energy of the moving plate that is absorbed by the metal foam layer was related to the densification of the foam on the collapse shock front, which is primarily characterized by the velocity and areal density of the impacting plate, by the initial density of the foam, and the density of the constituent material. For lower velocities, it was also characterized by the critical strain of the foam. It should be noted that the absorption energy was not characterized by the visco-plastic characteristics of the material.

Because the mechanism of energy absorption is related to the dynamics of the propagation of the collapsing wave, it is of interest to study the dynamic collapse behavior experimentally. In the past, a classical compression split Hopkinson pressure bar (SHPB) experimental procedure has been used in characterizing the high strain rate behavior of foam materials [3–9]. Testing of acoustically soft materials, e.g., foam, rubber, clay etc., using a traditional steel bar faces difficulties of

poor transmission to the transmitter bar (also known as the output bar). Use of aluminum and PMMA bars are common in the measurement of transmitted stress, and efforts in developing a Hopkinson bar test method for soft materials can be found [10,11]. Two other simple techniques for the dynamic testing of foam materials have been used: a direct impact single pressure bar technique and a rod impact (Taylor) testing technique [12–14]. In the direct impact single pressure bar technique (Fig. 2a), the specimen is placed on the impact end of the output bar and the striker bar (often called the projectile) is fired directly onto the specimen. This method requires a model to estimate the displacement of the impact on the face of the specimen.

Baker et al. [15] used a load cell to measure the force instead of using a single pressure bar in testing honeycomb materials. In this case, the kinetic energy of the projectile should be significantly smaller than the traditional SHPB, because the total energy required to collapse a small foam specimen is also very small. In the Taylor test technique, on the other hand, specimens can be fired at any impact velocity directly onto a rigid wall (Fig. 2b). A combination of Hopkinson bar and rod impact can also be used, where the foam specimen is fired directly onto a single pressure bar and is termed as 'Taylor cylinder–Hopkinson bar' test (Fig. 2c). This method also requires a model for the specimen deformation, while the force can be measured from the output bar signal. Following the analytical model and experimental procedure as described by Reid and Peng [1], Deshpande and Fleck [5] used a fixed mass (considerably bigger than the foam specimen) on the back of the specimen in measuring the force-time history in

aluminum alloy foams. The addition of a heavy mass in the back of the specimen adds complexity to the analysis; however, an ultra-light polymeric foam can be added to the back face of the specimen for stability during flight and the effect of the added mass can be neglected.

In this work, the direct impact of closed-cell aluminum foam cylinders onto the output bar in a single pressure bar set-up is considered. Unlike Deshpande and Fleck [5], and as mentioned above, an ultra-light polymeric foam attached to the back of the specimen is used, the mass of which is neglected to simplify the analysis. During the Taylor cylinder–Hopkinson bar impact tests, the acoustic signal generated in the output bar was registered and the samples were cross-sectioned along the central axis after recovery. The acoustic response of the system is obtained from the Hopkinson bar strain gage data and one can visually see the 'frozen' shock front in the specimen that stopped some distance from the contact surface, with said distance being dependent on the impact velocity of the foam cylinder. A theory, as well as numerical modeling, of this experiment are presented.

2. Quasi-static and impact testing of aluminum foam

Quasi-static compression and impact tests were conducted on cylindrical aluminum foam specimens, 19 mm in diameter and 40 mm in length. Test specimens were prepared by core-drilling a foam plate received from Fraunhofer Resource Center USA and manufactured by a powder metallurgical process developed by the Center. As a consequence of the manufacturing process, a dense Al skin (of average thickness 0.5 mm) is formed on the surfaces of the plate. Core-drilling was performed through the thickness of the plate and therefore specimens were essentially an aluminum cylinder foam core between two Al-discs. Before testing, samples were weighed and the average density of each specimen was calculated. Although the volume of the specimens were the same, the specimens were found to have a range of densities (0.35–0.39 g/cm^3) due to the non-homogeneous size and non-homogeneous spatial distribution of cells in a foam plate of dimension 300 mm × 300 mm.

A quasi-static compression test was conducted using a displacement controlled Instron test machine at a cross-head speed of 0.2 mm/s. From these tests, force–displacement curves were obtained and then stress–strain curves were calculated. Fig. 1 shows the quasi-static compression test results of three cylindrical specimens, where the compressive stress is presented as positive numbers. The stress–strain curve of individual foam samples (in the density range 0.351 to 0.385 g/cm^3) were similar; however, the variations in stress values are attributed to the variations in density, cell size, and
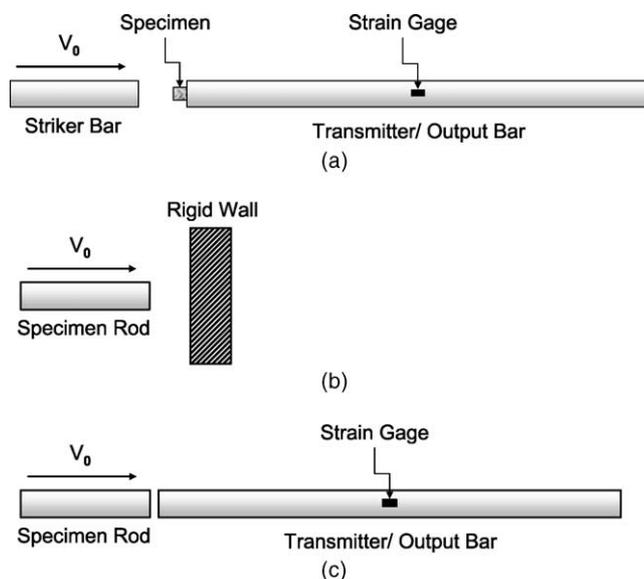

Fig. 2. Direct impact test methods for foam materials. (a) Single pressure bar, (b) rod impact (Taylor) test and (c) Taylor cylinder–Hopkinson bar test.

distribution. The same figure also shows the stress strain curve of a larger cubic sample (38 mm × 33 mm × 42 mm) with an average density of 0.33 g/cm³. Although this specimen has a lower average density than the core-drilled cylindrical specimens; in the plateau region, both specimen types showed similar stress values, and results have confirmed that the studied specimen size was sufficient to represent the bulk compression behavior. The plateau stress was not constant and increased continually as the strain increased as depicted in Fig. 1. Following the initial plateau stress of about 2 MPa, the stress increased to 4 MPa at 0.3 strain. At a strain of 0.4, densification started; and in this region, stress increased rapidly with increasing strain, which is a typical behavior of foam materials [16]. The average density, critical strain and stress, the densification strain, and elastic modulus for this foam material was found to be: $\rho_0 = 0.37$ g/cm³, $\varepsilon_{cr} = 0.008$, $\sigma_{cr} = 2.31$ MPa, and $\varepsilon_d = 0.51$, and $E_0 = 248$ MPa, respectively. The parameters for E-P-P-R model for this foam specimen was found to be: $\varepsilon_{max} = 0.863$, $\varepsilon_{cr}^P = 0.013$, $\sigma_{cr}^P = 4.03$ MPa, respectively, using Eq. (2).

Impact tests were performed by directly firing the foam specimens onto the impact end of the output bar of a single pressure bar configuration. Foam specimens were placed laterally inside the gas gun barrel with a polymeric foam backing, which was used to guide the foam sample in the barrel and provided a planar impact (Fig. 3). Prior to impact, near the impact area, the velocity was measured using an electronic velocity measurement unit consisting of two pairs of photodiodes and light sources. By varying the gas gun pressure, impact velocities in the range 20–200 m/s were obtained. The output bar is made from Inconel 718 alloy, 3620 mm in length and 19.05 mm in diameter. Other important properties of the bar are as follows: Young's modulus, 200 GPa, elastic wave speed, 4920 m/s and Poisson's ratio, 0.29. A full-bridge strain gage station on the bar was used to record the strain as a function of time. The strain gage data (volts) from the output bar is converted into stress and presented in Fig. 4 for three different impact velocities. The following relation is used

Fig. 3. Taylor cylinder–Hopkinson bar impact test of foam meterials in a single pressure bar test set-up.
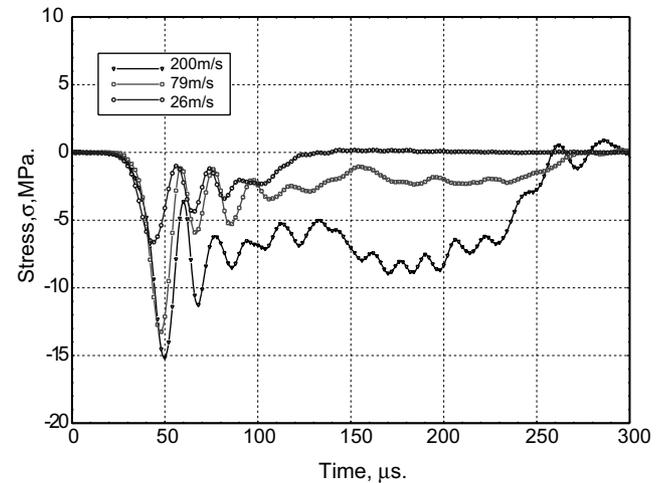

Fig. 4. Stress–time history of aluminum foam specimens fired at different impact velocities.

to convert the strain gage voltage into stress in the output bar:

$$\sigma(t) = \frac{E_B \cdot 2\varepsilon_V(t)}{G_g K_g V_I (1 + v_B)} \tag{3}$$

where, $\sigma(t)$ is the stress in the output bar as a function of time, $\varepsilon_V(t)$ is the strain gage voltage as a function of time, G_g is the amplification factor, K_g is the strain gage factor, V_I is bridge input voltage, E_B is the elastic modulus, and v_B is the Poisson's ratio of the bar material. The strain gage location on the output bar was 2712 mm away from the impact face, which introduced some dispersion (widening of stress pulse) in the stress responses. In addition to this effect, one observes some high frequency oscillations (a characteristic of the finite diameter Hopkinson bar [12]) in the responses too. In general, the stress responses have a sharp peak, followed by some oscillations and a long stress pulse (see, for instance, the 79 and 200 m/s impact velocity cases). These stress responses represent the stress pulse produced by the impact of a foam cylinder on the output bar. The zero in time scale on Fig. 4 is arbitrary and does not represent the time of impact of the foam specimen on the impact end of the output bar, because, the data acquisition was triggered by a single strain gage (quarter-bridge) located 172 mm ahead of the full-bridge strain gage station. The final length of aluminum foam specimens after impact are measured and sectioned. Fig. 5 shows the cross-sections of three specimens. At an impact velocity of 26 m/s, no shock front appeared and the specimen is almost un-deformed. At an impact velocity of 79 m/s, about half of the specimen is densified, and the shock front is clearly visible. At an impact velocity of 200 m/s, the foam specimen is almost completely collapsed. The cross-sections of the tested specimens also showed that there are variations in the
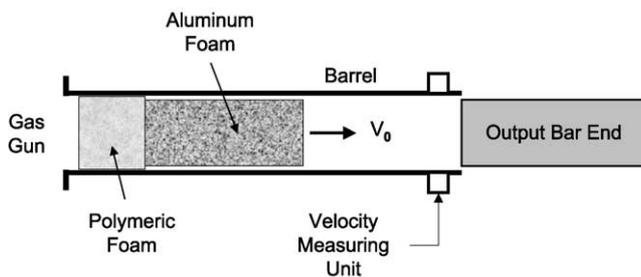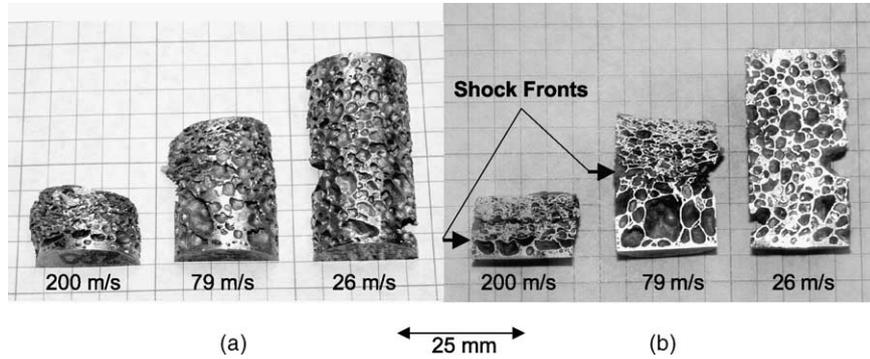
Fig. 5. Cross-sections collapsed of foam specimens. (a) Surfaces and (b) sections.

cell size and that may be responsible for the low frequency oscillations in the stress history as presented in Fig. 4. Future experiments should use larger diameter specimens to minimize the effect of cell size, which is not addressed in this study due to the limitation of the gas gun diameter. In order to get more insight into the experiments, a theoretical analysis, as well as numerical simulations, were conducted and described below.

3. Analytical consideration

The process of stopping a moving rod made from metal foam is physically more complex than stopping a plate with a foam layer, which was considered in a previous work [2]. As a preliminary exercise, consider the impact of an elastic body or rod on a rigid wall. After the impact, an acoustic stress wave starts to propagate in the opposite direction of the impact towards the free end of the elastic rod with the sound propagation velocity of the material. Ahead of this wave front, the material of the rod 'knows nothing' about the stress wave. Behind the moving front; the material is at rest, but stressed. When the wave front reaches the free end of the rod, the latter stops, and the whole rod is at rest. However, because the rod is stressed, the free end of the rod begins to move in the opposite direction with a velocity equal in magnitude to the initial one, and the reflected wave starts to propagate in the direction of the rigid wall. When this wave reaches the rigid wall, the rod loses contact with the wall and 'jumps off', as it were.

If the rod is made from metal foam, the situation is significantly different. When the rod impacts the wall and the dynamic pressure exceeds the critical stress, a shock wave will form in which the foam collapses. If the impact velocity is very low, and the dynamic pressure is well below the critical stress, the foam will remain elastic. The propagation dynamics of the stress wave will depend on what is happening prior to the wave front. If the velocity of the rod, V, exceeds the elastic wave speed of the foam, c_0, no signal can leave the shock wave front and the foam in front of the shock front stays completely unloaded and will continue to move with the initial velocity up to the moment when the entire rod will collapse. However, if the velocity of the rod is smaller than the elastic wave speed of foam, an acoustic precursor-elastic wave signal can propagate ahead of the collapse shock front. However, the stress due to the acoustic precursor cannot exceed the critical stress σ_{cr}^{P}. Following Taylor's rod impact theory [17], the material velocity after the acoustic precursor has passed will be equal to $(V - (\sigma_{cr}^{P}/\rho_0 c_0))$, and after the reflection of this wave from the free end, it will equal $(V - 2(\sigma_{cr}^{P}/\rho_0 c_0))$; ρ_0 being the initial density of the foam material. However, when the reflected wave reaches the front of the collapse, in the ideal case it cannot reflect back because it will be absorbed by the shock wave. Thus, after a time of order $2L_0/c_0$ (L_0 being the initial length of foam specimen), one can expect that some kind of quasi-static distribution of stress will form in this part of the rod. The simplest expression for the distribution of stress along the rod, considering the E-P-P-R model is

$$\sigma(x) = \frac{\sigma_{cr}^{P}}{L(t)} x \tag{4}$$

where x is the coordinate calculated from the free moving end of rod and $L(t)$ is the distance between the free end of the rod and the front of the collapse (Fig. 6). Then, suggesting that all parts of the rod before the collapse front are moving with approximately the same velocity (the difference is of order $2(\sigma_{cr}^{P}/\rho_0 c_0)$ which is small in comparison to V), the equation for the velocity of the rod goes as [12]

$$\rho_0 \dot{V} = \frac{\sigma_{cr}^{P}}{L(t)} \tag{5}$$

and the momentum continuity on the jump, mass conservation, and un-collapsed length are given, respectively, by

$$\rho_0 V(V + C) - \sigma_{cr}^{P} = -\sigma^{*} \tag{6}$$
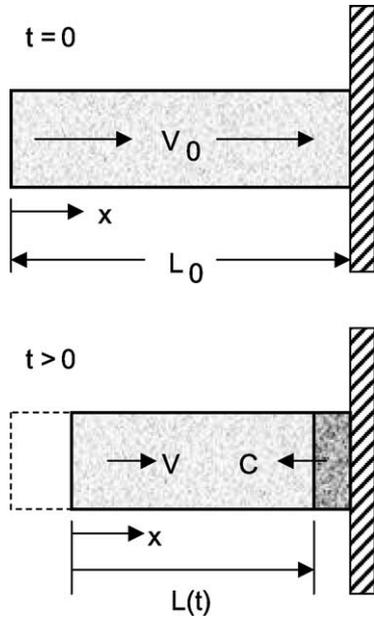
$$\rho_0 L(t) + \rho_a \int_0^t C \, dt = \rho_0 L_0 \tag{7}$$

Fig. 6. Cylinder impact model of foam materials.

$$L(t) = L_0 - \int_0^t (V + C)\, dt \tag{8}$$

where, C is velocity of shock front, σ^* is the stress in the densified region, ρ_0 and ρ_a are the densities of foam and aluminum, respectively. Consequently, from Eqs. (7) and (8) it can be shown that:

$$\dot{L} = \frac{dL(t)}{dt} = -\frac{\rho_a}{\rho_0} C \tag{9}$$

$$\dot{L} = -(V + C) \tag{10}$$

Thus

$$\frac{\rho_a}{\rho_0} C = V + C \tag{11}$$

and

$$V = \left(\frac{\rho_a - \rho_0}{\rho_0} \right) C \tag{12}$$

Substituting V in Eq. (5), the time derivative of C may be given as

$$\dot{C} = \frac{\sigma_{cr}^P}{(\rho_a - \rho_0) L} \tag{13}$$

Therefore

$$\ddot{L} = -\frac{\rho_a}{\rho_0} \dot{C} = \left(-\frac{\rho_a}{\rho_0} \right) \cdot \left(\frac{\sigma_{cr}^P}{(\rho_a - \rho_0) L} \right) \tag{14}$$

and finally

$$\ddot{L} = \frac{B}{L} \tag{15}$$

where

$$B = -\frac{\rho_a}{(\rho_a - \rho_0)} \frac{\sigma_{cr}^P}{\rho_0} \tag{16}$$

Eq. (15) can be solved as follows

$$\dot{L} \cdot \ddot{L} = \frac{B \cdot \dot{L}}{L} \tag{17}$$

and thus

$$\frac{d}{dt} \left[\frac{(\dot{L})^2}{2} \right] = \frac{d}{dt} (B \cdot \ln L) \tag{18}$$

leading to

$$(\dot{L})^2 = 2B \cdot \ln L + C_1 \tag{19}$$

the constant C_1 can be given via Eqs. (9) and (12), and thus

$$\dot{L} = -\frac{\rho_a}{\rho_a - \rho_0} V \tag{20}$$

If $t = 0$, one has $V = V_0$ and $L = L_0$. Thus

$$(\dot{L})_0 = -\frac{\rho_a}{\rho_a - \rho_0} V_0 \tag{21}$$

then one has

$$C_1 = \left(\frac{\rho_a}{\rho_a - \rho_0} \right)^2 V_0^2 - 2B \cdot \ln L_0 \tag{22}$$

and finally

$$\dot{L} = -\left(\frac{\rho_a}{\rho_a - \rho_0} \right) V_0 \sqrt{\left(1 + 2 \frac{B}{\left(\frac{\rho_a}{\rho_a - \rho_0} \right)^2 V_0^2} \cdot \ln \frac{L}{L_0} \right)} \tag{23}$$

or

$$\frac{1}{\sqrt{\left(1 + 2A \cdot \ln \frac{L}{L_0} \right)}} \frac{dL}{dt} = -\left(\frac{\rho_a}{\rho_a - \rho_0} \right) V_0 \tag{24}$$

This equation can be solved in terms of time as a function of L

$$t = -\left(\frac{\rho_a - \rho_0}{\rho_a} \right) \tau_0 \int_1^s \frac{ds}{\sqrt{(1 + 2A \cdot \ln s)}} \tag{25}$$

where

$$\tau_0 = \frac{L_0}{V_0} \tag{26}$$

$$s = \frac{L}{L_0} \tag{27}$$

and

$$A = \frac{B}{\left(\frac{\rho_a}{\rho_a - \rho_0} \right)^2 V_0^2} = -\frac{(\rho_a - \rho_0)}{\rho_a \rho_0} \frac{\sigma_{cr}^P}{V_0^2} \tag{28}$$

Denoting

$$u = \sqrt{(1 + 2A \cdot \ln s)} \qquad (29)$$

then

$$\ln s = \frac{u^2 - 1}{2A} \qquad (30)$$

or

$$s = \exp\left[\frac{u^2 - 1}{2A}\right] \qquad (31)$$

and thus

$$ds = \frac{u}{A} \exp\left[\frac{u^2 - 1}{2A}\right] du \qquad (32)$$

and the integral takes the form

$$t = -\left(\frac{\rho_a - \rho_0}{\rho_a}\right) \frac{\tau_0}{A} \int_1^s \frac{u \exp\left[\frac{u^2-1}{2A}\right] du}{u} \qquad (33)$$

It is important to mention that this solution remains valid only if $\sigma^* > \sigma_{cr}^P$. In the opposite case, no shock wave can appear. Expressing the material velocity V and front velocity C via $\dot{L}$, one has

$$C = -\frac{\rho_0}{\rho_a} \dot{L} \qquad (34)$$

$$V = -\frac{\rho_a - \rho_0}{\rho_a} \dot{L} \qquad (35)$$

and thus

$$\frac{\rho_0}{\rho_a}(\rho_a - \rho_0)(\dot{L})^2 + \sigma_{cr}^P = \sigma^* \qquad (36)$$

The physically meaningful solution for $\dot{L}$ gives the condition

$$\dot{L} < 0 \qquad (37)$$

and the critical point is

$$\dot{L} = 0 \qquad (38)$$

One can see that it is just the condition of the existence of a real solution (for $L < L_0$ or $s < 1$)

$$1 + 2A \cdot \ln s > 0 \qquad (39)$$

thus

$$\ln s_{cr} = -\frac{1}{2A} \qquad (40)$$

and

$$s_{cr} = \exp\left(-\frac{\rho_a \rho_0 V_0^2}{2(\rho_a - \rho_0)\sigma_{cr}^P}\right) \qquad (41)$$

with

$$L_{cr} = L_0 \exp\left(-\frac{\rho_a \rho_0 V_0^2}{2(\rho_a - \rho_0)\sigma_{cr}^P}\right) \qquad (42)$$

Thus, one can see that the length of the non-collapsed part of the rod is exponentially decreasing with increasing velocity of the foam rod, or decreasing critical
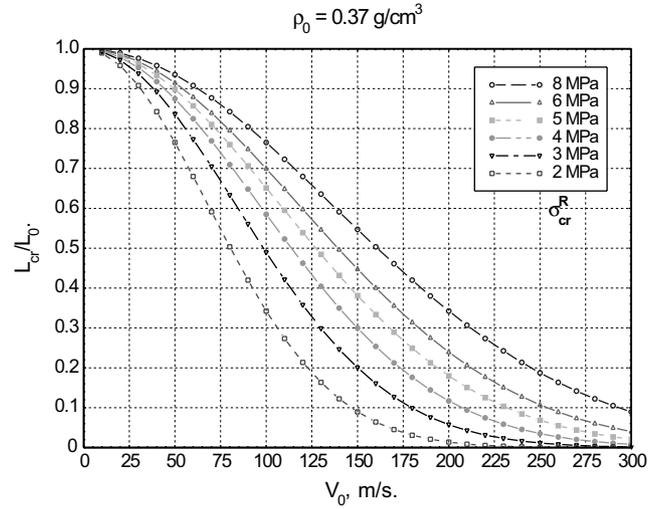

Fig. 7. Dimensionless critical un-collapsed length as a function of impact velocity and critical stress (E-P-P-R).

stress. It is assumed in the derivation of Eq. (42) that the critical stress, σ_{cr}^P, is not a function of impact velocity or strain rate. Fig. 7 shows the dimensionless critical un-collapsed foam length as a function of impact velocity for different values of σ_{cr}^P, at a constant foam density, $\rho_0 = 0.37$ g/cm^3. Similar plots can also be constructed using Eq. (42) for other foam densities, and can be used as a design chart for experiment. The main objective of the Taylor cylinder–Hopkinson bar impact experiment is to impact a specimen at a velocity such that the 'frozen' shock front is easily measurable. In order to experimentally measure the un-collapsed length with accuracy and to be able to differentiate between the critical stresses, one must choose a desired L_{cr}/L_0 value in the range 0.3–0.5 and choose the corresponding impact velocity. The experimentally measured value of L_{cr}/L_0 can then be plotted as a function of impact velocity and the data curve fitted using Eq. (42) to experimentally determine the E-P-P-R model parameter, σ_{cr}^P. Fig. 8 shows the experimentally measured values of L_{cr}/L_0 as a function of impact velocities. The critical stress, σ_{cr}^P, is found to be 3.92 Mpa, which agrees well with that estimated by using Eq. (2). The limited data presented in Fig. 8 shows significant scatter, however, it demonstrates the robustness of this simple experimental technique in obtaining the E-P-P-R model parameter, σ_{cr}^P, from simple measurements of the un-collapsed length, L_{cr}.

The present analytical model considered the displacement of the impact surface to be zero, as in the case of a rigid wall. However, in a real experiment the displacement of the impact wall or surface is not zero, but negligible in comparison to the total collapsed length of the foam specimen. The impact of the foam specimen on the Hopkinson bar impact face produces a stress wave that propagates along the bar. In order to get insight
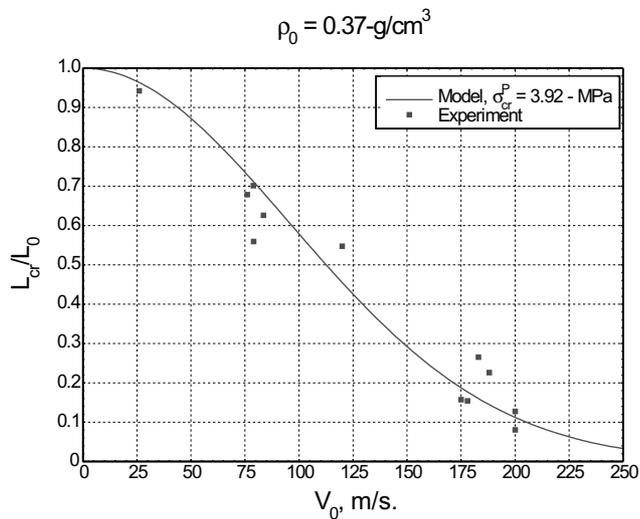
$\rho_0 = 0.37\text{-g/cm}^3$

Fig. 8. Experimantal dimensionless un-collapsed length as a function of impact velocity and E-P-P-R model fit.

into the stress wave propagation in the output bar, numerical experiments were conducted and are described below.

4. Numerical simulation of Taylor cylinder–Hopkinson bar impact experiment

A numerical simulation of the Taylor cylinder–Hopkinson bar impact experiment is performed using the explicit finite element code, LS-DYNA 960. A quarter symmetric three-dimensional numerical model of an aluminum foam specimen impacting on an output bar was developed. Boundary conditions representing two axes of symmetry are included in the model. A surface-to-surface contact condition is defined between the cylindrical aluminum foam specimen and the output bar end without friction. The impact velocity of the foam specimen is defined as the initial condition. Fig. 9 shows the finite element model of the Taylor cylinder–Hopkinson bar impact experiment. As described in the experimental section, the foam specimens have an aluminum skin of about 0.5 mm thickness. The present

model considers this feature by modeling a 0.5 mm aluminum skin on both sides of the specimen. Three elements are used through the thickness of the aluminum skin, which is the minimum geometric dimension (0.167 mm) of this model. In order to match the through-thickness fine mesh of the foam specimen, the mesh density along the length of the output bar is biased, such that both ends of the bar have similar element thicknesses. Linear elastic material properties ($E_B = 200$ GPa, $\rho_B = 8400$ kg/m³, $\nu_B = 0.29$) are used to model the Inconel output bar (MAT_ELASTIC). Although an elastic-perfectly-plastic-rigid (E-P-P-R) model for the foam is used in the analysis, to mimic a realistic stress wave experiments, the foam is modeled with the honeycomb material model available in LS-DYNA 960. MAT_HONEYCOMB allows one to use experimentally measured load curves in compression and shear. This material model neglects the elastic deformation and is good enough for the computation of energy and displacement; however, it is not good for the elastic stress analysis. The material parameters for aluminum foam used in the present numerical simulation are: foam density $\rho_0 = 370$ kg/m³, elastic modulus of un-collapsed foam, $E_0 = 248$ MPa, volume fraction of densified foam, $v_{f0} = 0.137$; while the deformation behavior is provided through load curves.

Load curves for all three directions are considered the same, and the shear behavior is considered as elastic-perfectly-plastic (Fig. 10). In addition to load curves, this model requires the elastic-plastic properties of fully compacted materials, and in the present case, the properties of aluminum ($E_a = 70$ GPa, $\rho_a = 2700$ kg/m³, $\nu_a = 0.285$, $\sigma_y^a = 240$ MPa) are used. The MAT_HONEYCOMB model [18] treats the material as isotropic or orthotropic before compaction, and the stress tensors are un-coupled with zero Poisson's ratio. After full compaction to final relative volume, the material is treated as elastic-perfectly-plastic. The details of the stress update equations can be found in [18]. Because the critical stress of the foam is much smaller than its constituent material, the skin is modeled with linear elastic properties of aluminum. The time increment in explicit integration is automatically calculated by LS-DYNA
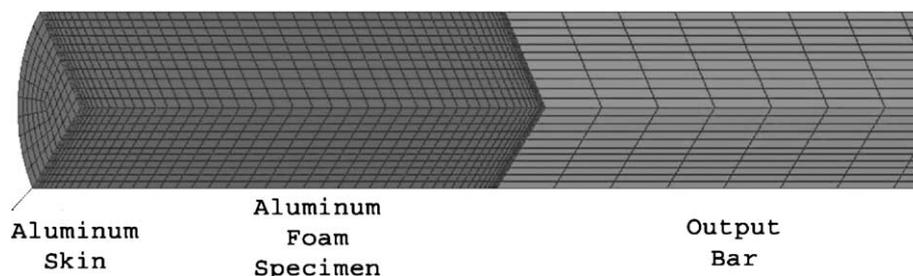

Fig. 9. Quarter-symmetric finite element model of the Taylor cylinder–Hopkinson bar impact test of aluminum foam specimen.
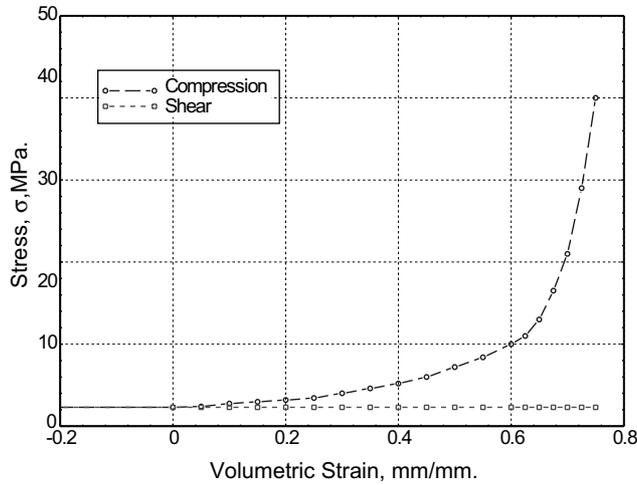
Fig. 10. Input load curves for aluminum foam taken from quasi-static compressive data.

Fig. 12. Comparison between experimental and numerical stress–time history.

960 for each element at each time step [19], and the minimum time increment (15 ns, first time step) of all elements is used.

Fig. 11 shows the stress–time history as obtained from the numerical simulation of the impact experiment described earlier. The time axis of the numerical response is shifted such that the rise of the first peak of the experiment matches with that of the simulation. Most of the features observed in the experiment are captured by the numerical prediction, e.g., the first peak, the Pochhammer modes, and the pulse duration. However, the predicted amplitude of the first peak and the trailing edge is higher than the experimental observations.

The experimental SHPB response for aluminum foam with an impact velocity of 79 m/s is compared with the numerical simulation in Fig. 12. The slope of the first peak matched well with the experiment, however, the amplitude is over predicted by a few percent. The total
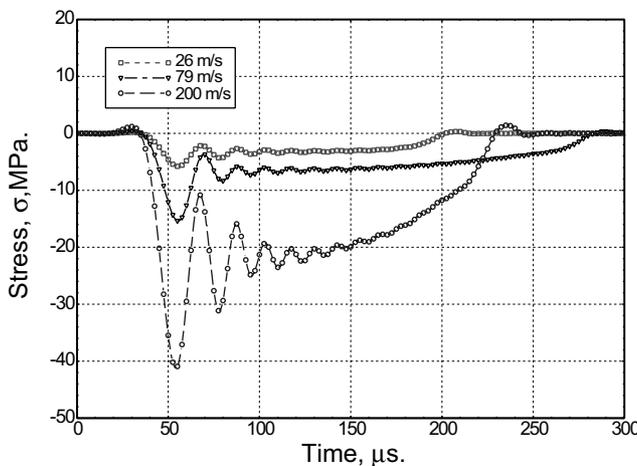
duration of the entire pulse matched well with the experiment. However, the amplitude of the trailing edge prediction is higher than the experimental observation. This can be explained by the non-uniform porosity and cell size distribution of the aluminum foam specimens, while the numerical simulation is based on uniform properties.

In order to understand the impact response of the aluminum foam specimens, a parametric study is performed using the finite element model. It was mentioned earlier that the finite element model of the foam specimen consists of two half-mm thick aluminum skins. The first parametric study involves just impacting an aluminum skin onto the output bar at an impact velocity of 79 m/s. The second parametric study involves changing the aluminum skin properties into foam properties, which will simulate the impact of a pure aluminum foam specimen on the output bar. Fig. 13 presents the output bar responses of all the test cases at 79 m/s impact velocity. The impact of an aluminum skin produced a short pulse, the frequency and amplitude of which are very similar to the first peak of the aluminum foam specimen with skin. This parametric study indicates that the first peak obtained from the experiment is due to the presence of an aluminum skin on the foam specimen. The numerical response of aluminum skin is subtracted from the numerical response of the aluminum foam specimen with skin (Foam with Al-Skin minus Al-Skin), which shows good correlation with the numerical response of aluminum foam without skin (All Foam). It is thus very important to remove the aluminum skins from the foam specimen to avoid high frequency oscillations, which complicates the data interpretation. If the first peak is associated with the response of the aluminum skin, then the trailing edge of the stress–time data represents the dynamic stress developed in the collapsed part of the specimen.

Fig. 11. Numerical stress–time history of aluminum foam specimens with different impact velocities.

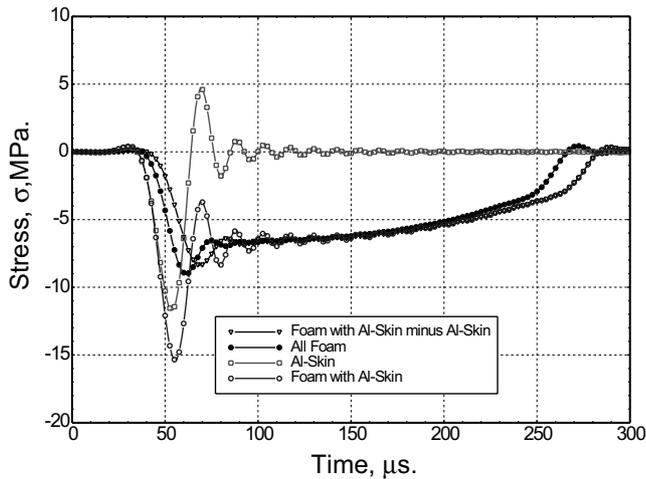Fig. 13. Effect of aluminum skin on the stress–time history.

The dimensionless change in the length, $\Delta L/L_0$, of the aluminum foam specimens under impact is computed by dividing the difference in displacements of the specimen edges by its original length, L_0. Fig. 14 shows that $\Delta L/L_0$ is almost linear up to the point where the deformation of aluminum foam stops. These constant $\Delta L/L_0$ values are compared with the measured final change in length values after the impact experiments (solid lines with corresponding experimental measurements marked). For small deformations, the numerical prediction matches well with the experimental values; however, it does not show good correlation in the case of large deformation. This can again be attributed to the non-uniform distribution of foam porosity, because the large deformation experiments showed non-uniform deformations of the specimens (impact velocities 79 and 200 m/s in Fig. 6) as discussed in the analytical section, while the numerical analysis considers the porosity as uniform.
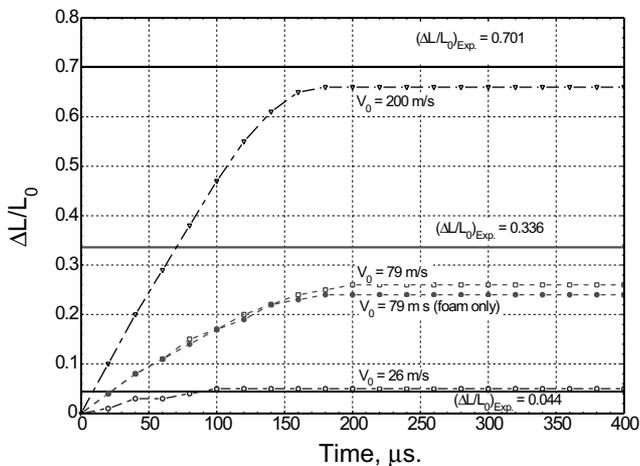

Fig. 14. Dimensionless change in length–time history of the aluminum foam specimens at different impact velocities.

5. Summary

It has been shown that the Taylor cylinder–Hopkinson bar impact experiments with metal foam are a simple and reliable method for the investigation of the non-equilibrium deformation of the foam under fast shock. As in the Taylor impact experiment, the length of the un-loaded end of the sample after the impact, can be used for investigating the dynamic deformation of the foam under impact and can be correlated with the critical stress of E-P-P-R model. The analytical solution for the critical un-collapsed length can be used to create design charts for experimental design. Because of the exponential dependence on the inverse of the critical stress of the length of the non-deformed end of the specimen, analytical and numerical modeling shows that this experimental technique can be used for a precise investigation of the dynamic critical stresses. Numerical simulation provided insight into the effect of the aluminum skin on the foam specimen and helped specimen design for future experiments. Further development of this technique will allow the determination of the rate dependent critical stress of porous foam type materials.

References

[1] Reid SR, Peng C. Dynamic uniaxial crushing of wood. Int J Impact Eng 1997;19(5-6):531–70.
[2] Lopatnikov SL, Gama BA, Haque Md.J, Krauthauser C, Gillespie Jr. JW. Non-equilibrium dynamic deformation and energy absorption of metal foams: high-velocity plate impact, Int J Impact Eng, submitted.
[3] Yi F, Zhu Z, Hu S, Yi P, He L, Ning T. Dynamic compressive behaviour of aluminum alloy foams. J Mater Sci Lett 2001; 20(18):1667–8.
[4] Zhao H, Gary G. Behaviour characterisations of sheet metals, metallic honeycombs and foams at high and medium strain rates. Key Eng Mater 2000;177–180(1):225–30.
[5] Deshpande VS, Fleck NA. High strain rate compressive behaviour of aluminum alloy foams. Int J Impact Eng 2000;24(3): 277–98.
[6] Kanahashi H, Mukai T, Yamada Y, Shimojima K, Mabuchi M, Nieh TG, et al. Dynamic compression of an ultra-low density aluminum foam. Mater Sci Eng A 2000;280(2):349–53.
[7] Dannemann KA, Lankford Jr J. High strain rate compression of closed-cell aluminum foams. Mater Sci Eng A 2000;293(1): 157–64.
[8] Mukai T, Kanahashi H, Miyoshi T, Mabuchi M, Nieh TG, Higashi K. Experimental study of energy absorption in a close-

celled aluminum foam under dynamic loading. Scr Mater 1999;40(8):921–7.

[9] Mukai T, Kanahashi H, Yamada Y, Shimojima K, Mabuchi M, Nieh TG, et al. Dynamic compressive behavior of an ultra-lightweight magnesium foam. Scr Mater 1999;41(4):365–71.

[10] Chen W, Lu F, Zhou B. Quartz-crystal-embedded split Hopkinson pressure bar for soft materials. Exp Mech 2000;40(1):1–6.

[11] Chen W, Zhang B, Forrestal MJ. Split Hopkinson bar technique for low-impedance materials. Exp Mech 1999;39(2):81–5.

[12] High strain rate tension and compression tests. ASM handbook volume 8. Mechanical testing and evaluation, ASM International; 2000.

[13] Meyers MA. Dynamic behavior of materials. John Wiley and Sons Inc.; 1994.

[14] Johnson W. Impact Strength of Materials, London, Edward Arnold, New York, Crane, Russak, 1972.

[15] Baker WE, Togami TC, Weydert JC. Static and dynamic properties of high-density metal honeycombs. Int J Impact Eng 1998;21(3):149–63.

[16] Gibson LJ, Ashby MF. Cellular solids—structure and properties. 2nd ed. Cambridge University Press; 1997.

[17] Taylor GI. The use of flat-ended projectiles for determining dynamic yields stress I. Theoretical considerations. Proc Roy Soc London A 1948;194:289.

[18] LS-DYNA Keyword User's Manual, Version 960, LSTC, Livermore, CA, 2001.

[19] Hallquist JO, LS-DYNA Theoretical Manual, LSTC, Livermore, CA, 1998:19.1–19.2.